http://dx.doi.org/10.5012/bkcs.2013.34.7.2155

Fabrication of CNT/CMK3 Carbon Composites with High Electrical/Thermal Conductive Properties

Seung Dae Choi, Ju Hyun Lee, Da Min Park, and Geon-Joong Kim*

*Department of Chemical Engineering, Inha University, Incheon 402-751, Korea. *E-mail: kimgj@inha.ac.kr*
Received February 26, 2013, Accepted April 26, 2013

Composite materials of mesoporous carbon and carbon nanotubes were synthesized using Ni, Co and Pd-loaded CMK3 *via* a catalytic reaction of methane and CO_2. The CNTs grew from the pores of the mesoporous carbon supports, and they were attached tightly to the CMK3 surface in a densely tangled shape. The CNT/CMK3 composite showed both non-graphitic mesoporous structures, and graphitic characteristics originating from the MWCNTS grown in the pores of CMK3. The electrochemical properties of the materials were characterized by their electrorheological effects and cyclic voltammetry. The CNTs/CMK3 composites showed high electrical conductivity and current density. The CNT/CMK3 or KOH-modified CNT/CMK3 particles were incorporated in a PMMA matrix to improve the thermal and electrical conductivity. Even higher thermal conductivity was achieved by the addition of KOH-modified CNT/CMK3 particles.

Key Words : Carbon composite, CNT, Mesoporous carbon, Electrical conductivity, Electrode material

Introduction

The electrochemical capacitor is one of the important components in high power electric devices used for the development of hybrid vehicles. Supercapacitors (SCs) have attracted considerable attention in recent years due to the increasing demand for novel electrical energy accumulators with a high specific power and durability.[1] These devices are particularly suited for applications where the energy should be delivered in pulsed mode with a discharge duration ranging from few milliseconds to few minutes. As examples, SCs are currently using in aircraft emergency doors and slide actuation systems, and are perfect companions of regular batteries for electricity powered vehicles at start-up or speed-up.[2]

Carbon-based pseudo-capacitor electrode materials have been used to store the charges *via* fast Faradaic reactions and also by double-layer charging. Accordingly, carbonaceous materials such as carbon nanotubes (CNTs)[3-7] and mesoporous carbon (MC),[8-11] have been used widely as the electrode materials of electric double layer type capacitors (EDLCs) because of their high chemical and physical stability, good conductivity, and availability. To achieve high performance as SCs, both micro- and meso-pores should be formed in the carbon matrix to provide high surface areas, which plays an important role in charging the electrical double layer and providing easy electrolyte diffusion for accessibility.[8,12] Most activated carbon commercially available contains micropores, allowing only slow ion transportation rates through the small pores. On the other hand, the presence of interconnected regular mesopore channels and secondary micropores probably makes the surface of MC favorable for charging the electric double-layer through improved electrolyte transport.[7-11]

The recent applications of CNTs as an electrode material focused on their microscopic and macroscopic porous structures and electrochemical behavior.[13-18] The CNT electrodes exhibit unique pore structures and high use efficiency of specific surface areas.[15,17] The CNT electrodes for EDLCs have excellent absorption characteristics owing to the accessible mesopores formed by the entangled individual CNTs.[15,18] An enhancement of the specific capacitance given by CNTs was achieved by mixing with conducting polymers. An *et al.*[19] fabricated nanocomposite electrodes of single-walled CNTs and polypyrrole to enhance the specific capacitance of SC. The improved effects of the conducting agent added to the nanocomposite electrodes on the specific capacitance and the internal resistance of SCs have been investigated.

The modification of the CNTs[1,3,20] or MC[21,22] using a specific additive to provide a quick pseudocapacitive material, such as RuO_2 and MnO_2, is another route for enhancing the capacitance. Park *et al.*[21] reported on the preparation of RuO_2 nanoparticles dispersed in CNTs along with their performance as active materials in electrochemical capacitors. Ko and Kim[3] prepared chemically activated multi-walled CNTs (A-CNTs) using KOH, and used it as an additive in the fabrication of MnO_2 electrodes to enhance the performance of MnO_2-based SCs. The MnO_2/A-CNT composite electrode exhibited improved capacitance, showing 250 F/g at scan rates of 10 mVs^{-1}, compared to 215 F/g for the MnO_2/CNT composite electrode.

As an example of the modified MC electrode, Dong *et al.*[22] presented an *in situ* reduction method to synthesize a MnO_2/MC composite (MnC). They obtained a large specific capacitance of more than 200 F/g for a MnC composite with high electrochemical stability and reversibility. Lei *et al.*[2] suggested that the electrochemical performance could be improved by the deposition of a controlled thickness of MnO_2 on the carbon surface with interconnected large meso-

pores. One approach to enhancing the specific capacitance of an electrode can be the conjunction of CNT into the CMK-3 substrate. CNTs can be grown by the catalytic reaction of methane on Ni metal particles immobilized at the mesopore channels of CMK-3.

In this study, CNT/CMK-3 carbon composites were prepared and their electrical and thermal conductivity were examined. The MWCNT/CMK-3 composite showed high electrical and thermal conductivity in the polymer matrix. In addition, the effects of the metal catalyst type, such as Ni, Co and Pd, and the metal content on the structure of the CNTs grown on CMK-3 were examined in detail. The electrochemical performance was expected to be improved by several material design parameters including the properties of CNTs, and the porosity of CMK-3 allowing electrolyte accessibility. Therefore, in this study, CNT/CMK-3 composites were modified with KOH to develop additional pores, and their physical and electrochemical characteristics were investigated and compared with those of unmodified CNT/CMK-3.

Experimental

Synthesis of Mesoporous Silica Template and Mesoporous Carbon. C-SBA-15 was synthesized using SBA-15 silica as the template and sucrose as the carbon source. A high quality SBA-15 sample was prepared using a triblock copolymer, EO_{20}-PO_{70}-EO_{20} (Pluronic P123, Aldrich), as the surfactant and tetraethylorthosilicate (TEOS, 98%, Aldchich) as the silica source, by modifying the synthetic procedure reported by Zhao *et al*.[11] The starting composition for the synthesis of high grade SBA-15 was 1.72 mol of P123, 0.10 mol of TEOS, 0.60 mol of HCl and 20 mol of H_2O.

The aqueous solution of sucrose mixed with a sulfuric acid was introduced to the calcined SBA-15 in a similar method to the synthesis of CMK3[23] except for different amounts of sucrose and H_2SO_4. As a typical method, 1 g of SBA-15 was added to a solution obtained by dissolving 1.25 g of sucrose and 0.14 g of H_2SO_4 in H_2O (5 mL). Detailed procedures to obtain the mesoporous carbons were followed the method described by Jun *et al*. Carbonization was completed by pyrolysis of the sample at temperatures of up to 900 °C under an inert nitrogen atmosphere. The carbon-silica composite obtained after pyrolysis was washed with 5 wt % HF at room temperature, to remove the silica template.

Composites of Mesoporous Carbon (CMK3) and MWCNTs. The CMK3 support was impregnated with an ethanol solution of nickel nitrate at a specific concentration (5-30 wt %) at room temperature, filtered, washed with ethanol, and dried at 300 °C for 12 h. The sample was used to synthesize the CNTs without further treatment. The mass fraction of Ni in the Ni/SBA-15 catalyst is in the range of 30 wt %. Ni-loaded CMK-3 (1.0 g) was placed into a quartz tube. The catalyst was pretreated at H_2 at 700 °C for 2 h, and then heated to 900 °C under a CH_4 (50 sccm) and H_2 flow (100 sccm). After a certain reaction time (30 min), the system was cooled to room temperature by H_2. A composite of the MWCNTs and CMK3 was treated 3 times with a HF solution (10 wt %) to remove the Ni metals from the carbon materials. Scheme 1 summarizes the method for fabricating the carbon composites. The samples of the MWCNTs and CMK3 composite are designated as CNT/CMK-3. In addition, the carbon samples were treated with a 20-30 wt % KOH solution and calcined in a N_2 stream at 800 °C to produce extra pores in the walls.

Characterization. X-ray powder diffraction (XRD, D/MAX 2500V/PC) of the parent mesoporous silica, SBA-15, and its carbon replica material (CMK3) was obtained using Cu Kα radiation. The data was collected from 0.7 to 3° (2θ) with a resolution of 0.02°. The morphology and microstructures of the as-prepared samples were characterized by field emission transmission electron microscopy (FE-TEM, S-4200), and field emission scanning electron microscopy (FE-SEM, JEM-2100F). Nitrogen adsorption/desorption analysis was performed at −196 °C using a surface area and porosity analyzer (Micromeritics, ASAP 2010). The sample was outgassed at 10^{-5} torr and 200 °C before the measurements. The specific surface areas were calculated according to BET theory, and the mean pore size was determined by BJH analysis. The electrochemical properties of the samples were tested by cyclic voltammetry (Autolab 128N). The electrorheological (ER) properties of the fluid containing the metal microspheres were examined under an electric field of 1.4 KV/min in silicon oil (10 vol %). The thermal conductivity of the prepared PMMA pads containing pure CNT, CMK3 or CNT/CMK3 composites were measured using QTM-500 (Kyoto Electronics, Japan). QTM-500 measures the thermal conductivity of the thick and thin samples quickly using a hot wire method.

Results and Discussion

The physical properties of the SBA-15 silica, CMK3 and

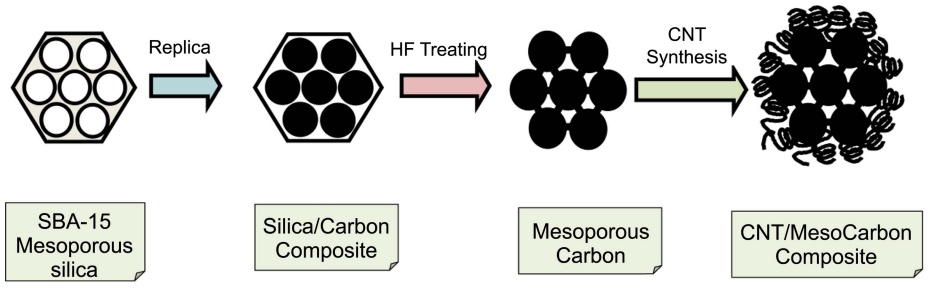

Scheme 1. Synthetic procedure of CNT/CMK3 composite.

CNT/CMK3 composite were investigated using a range of techniques. The presence of mesopores in the CMK3 and CNT/CMK3 is supported by XRD, TEM and N_2 adsorption analysis. The ordered arrangement of mesopores in the synthesized carbon replica (CMK3) from SBA-15 silica showed well-resolved XRD peaks, as shown in Figure 1, which can be assigned to the (100), (110) and (200) diffraction planes of the 1-D hexagonal space group (*p6mm*); similar to the case of the starting SBA-15 silica mold. CNT/CMK3 also showed similar diffraction peaks to CMK3 but with a weaker intensity. This suggests that the ordering of the hexagonal array of the CMK3 mesostructure decreased because of the incorporation of MWCNTs inside the mesopores of CMK3.

The XRD patterns over the wide-angle region (10-90°) allowed an assessment of the graphitic nature of the carbon synthesized. As shown in Figure 1(b), pure CNTs show well-defined XRD peaks at approximately 26 and 44° (2θ), which can be assigned to the (002) and (100) diffractions of the graphitic framework.[35] In contrast, the XRD pattern of CMK3 derived from glucose and sulfuric acid are characteristic of amorphous carbon, suggesting difficult graphitization of the frameworks. Carbon with good electronic conductivity with a large surface area is desirable for certain emergent applications, such as SC and catalytic supports in fuel cell systems. On the other hand, the carbon materials exhibiting these characteristics are difficult to synthesize.[24] Although the graphitic carbon derived from certain polymers or mesophase pitch showed good electrical conductivities, they are unsuitable for developing porosity due to the activation procedures. Therefore, porous carbon was obtained from non-graphitizable materials in general. Consequently, they cannot achieve high electrical conductivity even after heat treatment at high temperatures.[24]

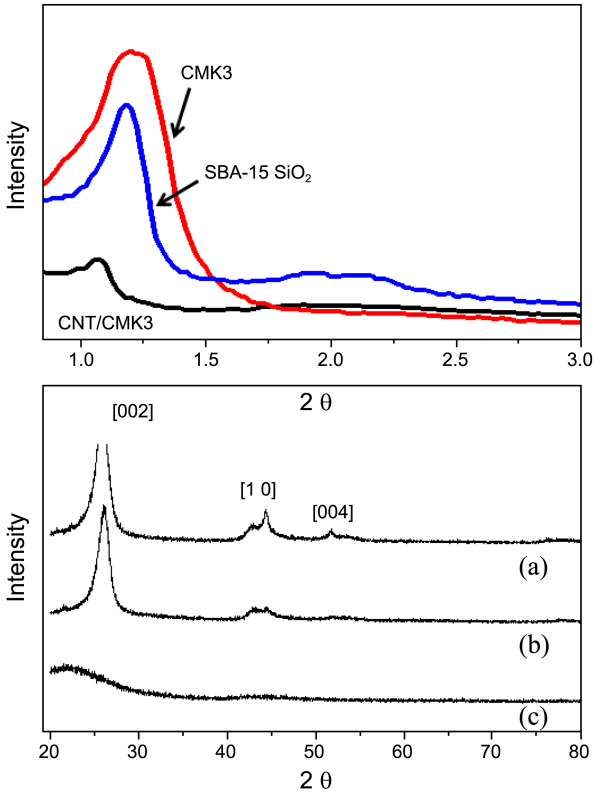

Figure 1. X-ray powder diffraction of CNT (a); CNTs/CMK3 (b); CMK3 (c).

The carbon CNT/CMK3 composite samples exhibited both regular mesopore structures, and the graphitic characteristics originated from MWCNTS grown in the CMK3 pores. This material is expected to be a good candidate for use in electronic conductors and electrodes.

The effects of metal amount loaded on CMK3 and metal types on the morphology of product fibrous carbons were examined by SEM. The morphology of CMK3 in Figure 2(b) is similar to that of silica SBA-15 (Fig. 2(a)), indicating carbonization through the reverse replication to form mesopore channels. The SEM images in Figure 2 shows that the as-synthesized CMK3 sample consists of many rope-like domains with relatively uniform sizes of ~2 μm, which are aggregated into wheat-like macrostructures. The CNTs were attached to each other in a densely tangled shape on the surfaces of CMK3. Figure 2 shows that the MWCNTs grew over the entire range of mesopores in CMK3. As many end parts of CNTs were embedded strongly in the pores of CMK3, they were bound tightly to the mesoporous carbon surfaces after washing and sonication in a solvent.

Figure 3 shows TEM images of SBA-15 silica, CMK3 and CNT/CMK3 viewed along or perpendicular to the direction of the hexagonal pore arrangement. The mesopore structure of CMK3 (Fig. 3(b)) was a precise inverse replica of SBA-15 silica (Fig. 3(a)). The TEM image at high magnification showed well defined mesopore structures in the CMK3 samples before and after the loading of Ni. The high-resolution TEM images showed that Ni metals were dispersed well as nanoparticles in the pores and the MWCNTs were grown well from the pores of CMK3. The CMK3 matrix and grown CNTs were combined tightly. The Ni nanoparticles existed

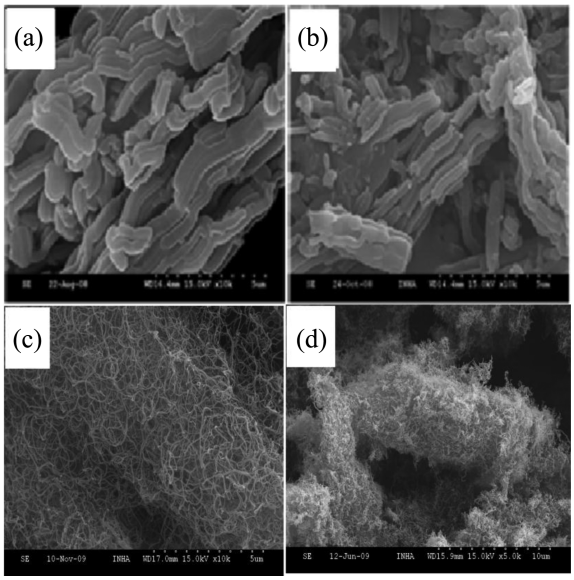

Figure 2. SEM images of silica SBA-15 (a), CMK3 (b), and CNTs/CMK3 (c, d). 15 wt % Ni metal (c) and Co metal (d) were used as a catalyst for the synthesis of CNTs, respectively.

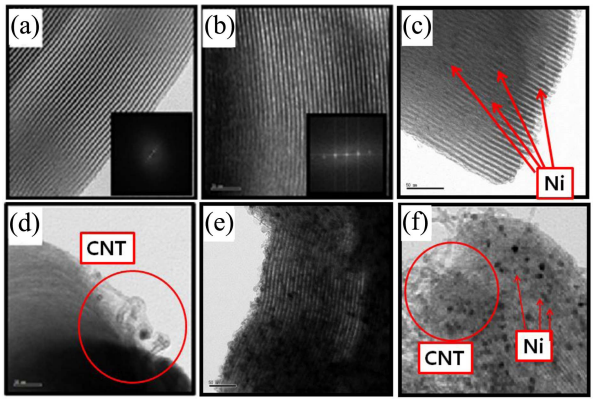

Figure 3. TEM images of silica SBA-15 (a), CMK3 (b), 5 wt % Ni loaded CMK3 (c), 5 wt % Ni loaded CNT/CMK3 (d), 15 wt % Ni loaded CMK3 (e) and 15 wt % Ni loaded CNT/CMK3 (f).

at the one tip of the carbon fibers, and the other part of CNT bundles were implanted in the pores of CMK3, as shown in Figure 3(d) and 3(f).

The effects of the Ni, Co and Pd loading used to fabricate the CNTs on the morphology of the fibers produced were examined by SEM and TEM. The apparent tangled shape of the fibers was similar to that in Figure 4(a), (d) and (g), but their microstructures were quite different depending on the Ni loading. When 5 wt % Ni was loaded on CMK3, no severe Ni sintering was observed during CNT growth at high temperatures (*e.g.* 900 °C). The particle size of Ni present at the tip of CNT was approximately 5 nm. On the other hand, as the Ni content was increased to 30 wt %, the initially small Ni particles (5-8 nm; Fig. 3(e)), which had been reduced at 450 °C, grew to larger than 30 nm during the fabrication of CNTs (Fig. 4(h)). In addition, the mean diameter of the crooked CNTs increased from 20 to 40 nm with increasing Ni content from 5 to 30 wt %. TEM revealed multi-walled CNTs and graphitic sheets in the wall layers. The number of graphitic layers in the CNT walls increased from 15 to 40 with increasing Ni content from 5 to 15 wt %

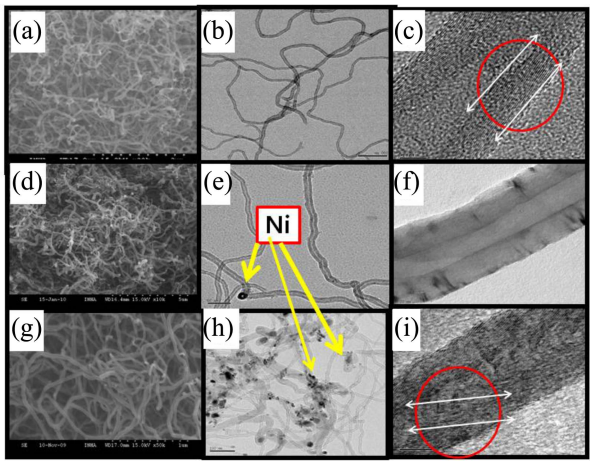

Figure 4. SEM images of carbon tubes fabricated on 5 wt % Ni/CMK3 (a), 15 wt % Ni/CMK3 (b), 30 wt % Ni/CMK3 (c) and TEM photographs for CNTs synthesized by 5 wt % Ni (b, c), 15 wt % Ni (e, f) and 30 wt % Co (H, I) on CMK3.

(Fig. 4(c) and 4(f)). The sharp strips between the graphitic sheets indicated their good crystallinity at a 5 wt % and 15 wt % Ni loading, showing the horizontal stacking of graphitic sheets. On the other hand, under a higher Ni loading (*e.g.* 30 wt %), some section-sealed structures were observed inside the carbon tubes. The diameter of the interior vacant channel became narrow (1-3 nm) (Fig. 4(i)). This material was not a tube, but rather a fiber. In particular, in this case, the graphitic layers of the walls were stacked at inclination angles of 45° (Fig. 4(i)).

Figure 5 shows the effects of the Co metal content on the morphology of CNTs synthesized at 900 °C by a reaction of methane and carbon dioxide. The mean diameters of the CNTs increased with increasing cobalt content. Most CNTs tangle together on the mesoporous CMK3 substrate, as shown in Figure 5(a) and 5(b). When the cobalt content was 5 wt %, the CNTs had an outer diameter of ~20 nm with a wall thickness of 8-10 nm, as shown in Figure 5(c). On the other hand, as the Co metal content was increased to 30 wt %, CNTs with uneven diameters and very thick walls formed, and the vacant inside was plugged in a similar manner to that observed with the Ni metal catalysts (Fig. 5(d) and 5(e)). Because the quality of CNT fabricated by Ni was better than that by Co metal, the CNT/CMK3 system using 5% Ni metal was selected mainly to further examine the electrical and thermal properties of the samples.

The effects of the Pd loading on the morphology of the carbon fibers produced were examined by SEM and TEM. Figure 6 lists the apparent tangled shape of the product fibers on CMK3. Their microstructures were similar, even with a different Pd loading. On the other hand, the mean diameter of the carbon fibers was similar at 35 nm at Pd loadings of 5-30 wt %. In particular, using Pd metals as a catalyst for the synthesis of CNTs, carbon fibers were formed instead of carbon tubes; no vacant channels were observed in the carbon bodies (Fig. 6(b), (c) and (d)). The graphitic layers in the fiber walls were stacked at inclined angles.

Figure 7 shows N_2 adsorption isotherms for CMK3 and CNT/CMK3 compared to the parent SBA-15 silica, respec-

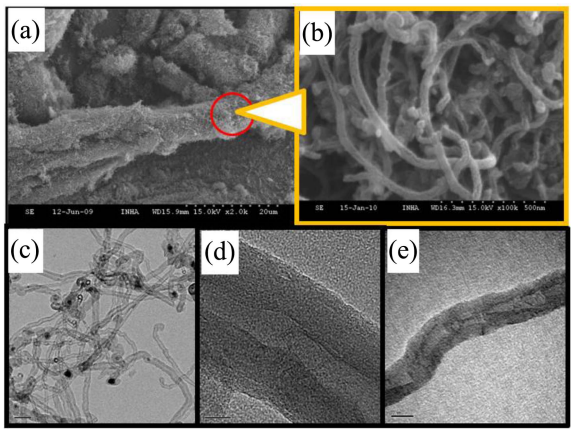

Figure 5. SEM images of carbon tubes grown on 30 wt % Co/CMK3 (A and B) and TEM photographs for CNTs synthesized by 5 wt % Co (c), 15 wt % Co (d) and 30 wt % Co (e) on CMK3.

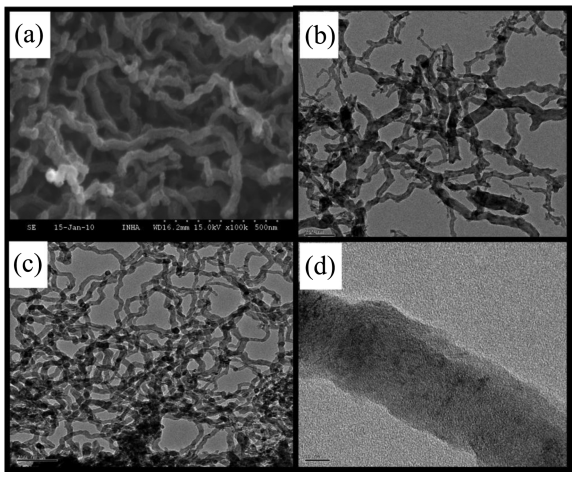

Figure 6. SEM and TEM images of carbon fibers grown on 5 wt % Pd/CMK3 (a; SEM, b; TEM) and 20 wt % Pd/CMK3 (c and d).

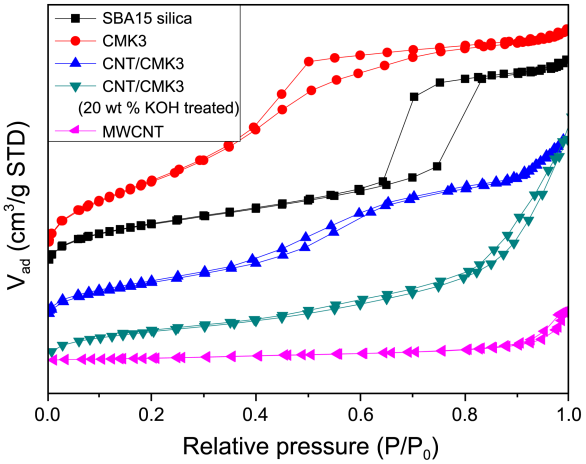

Figure 7. Nitrogen adsorption/desorption isotherms of SBA-15 silica, MWCNT, CMK3, and CNT/CMK3 composites.

tively. The N_2 adsorption/desorption isotherms of all three samples (Fig. 7(a)) were the H_1-type hysteresis loop, which is typical for mesoporous materials with ordered cylindrical channels. The N_2 adsorption result also suggests that CMK3 was mostly mesoporous with a narrow pore-size distribution of 4.6 nm. In contrast, the pore size distribution of SBA-15 was centered at 6.8 nm. The mean pore size of CNT/CMK3 (2.7 nm) was 1.9 nm lower than the diameter of carbon CMK3. The pore volume of SBA-15, CMK3 and CNT/CMK3 were 1.3, 1.7 and 1.0 cm^3 g^{-1}. The mesoporous CMK3 had a high surface area of 1200 m^2/g, but that of CNT/CMK3 decreased to 500 m^2/g. This suggests that some of the MWCNTs existed in the pores of CMK3, partially blocking the pore entrance. The surface areas of carbon materials increased after KOH modification followed by thermal activation at 800 °C. The KOH-modified CNT showed a higher BET surface of 200 m^2/g than a fresh CNT (100 m^2/g). Similarly, for CNT/CMK3, the BET surface area increased to 750 m^2/g after the KOH treatment.

Raman spectroscopy was used to characterize the carbon products and examine the defect and quality in the structures. The band at 1590 cm^{-1} (so-called G-graphite band) was assigned to one-phonon zone-center Raman scattering in graphite. Another Raman peak, which is typical for graphitic materials in the vicinity of 1290 cm^{-1}, was as assigned to the D-disorder-induced mode. The light scattering on phonons with non-zero k-vectors contributes to this D-signal, whose intensity increases with increasing number of defects in the graphite lattice.[25]

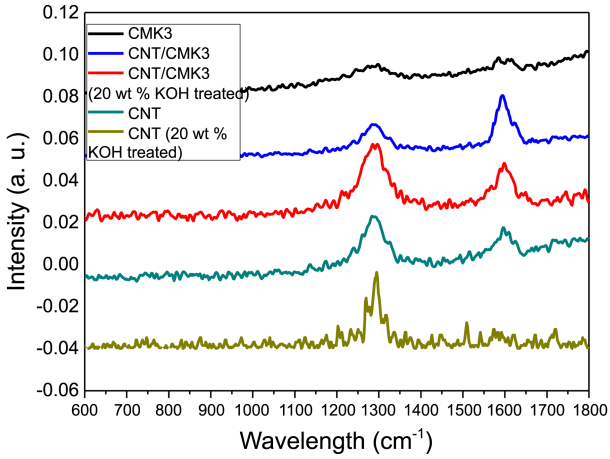

Figure 8. Raman spectra of commercial MWCNT, CMK3, CNT/CMK3 composite and 20 wt % KOH modified carbon samples.

A previous paper reported that the G-band of CNTs decreased gradually with increasing metal content in the both cases of Ni and Co metals.[26] The CMK3 sample showed very weak peak intensity for both D- and D-bands (Figure 8), indicating the characteristics of amorphous carbon. A more highly graphitic structure was formed for the CNTs compared to CMK3, showing higher peak intensities of the G- and D-bands. On the other hand, the CNT/CMK3 composite showed two strong peaks on the Raman spectrum, which is similar to those of the CNTs, as shown in Figure 8. This improvement in the graphitic nature of the CNT/CMK3 composite was attributed to the incorporation of CNTs. Furthermore, when the carbon was treated with 20 wt % KOH and calcined at 800 °C for activation, both CNT and the CNT/CMK3 composite showed a loss of graphitic ordering, which manifested as a decrease in the G-band and an increase in the D-band. KOH modification causes many structural defects in the carbon matrix with the formation of extra pores during activation.

The electrical conductivity of the composites was examined by observing the ER effects. The ER fluids were prepared by sonication using the dried composites of mesoporous carbon and CNTs dispersed in silicone oil (10 vol %). No stabilizers were added to the mixture. An AC high voltage source was used to apply a voltage to the sample. The gap between the two parallel electrodes was fixed to 350 m. Microstructural images of the ER fluid were obtained by optical microscopy as shown in Figure 9. The behavior of the particle chain (so called "fibrillation") was observed under an applied electric field (1.4 kV/ mm) for 5 sec based on interfacial polarization of the composites in silicone oil.

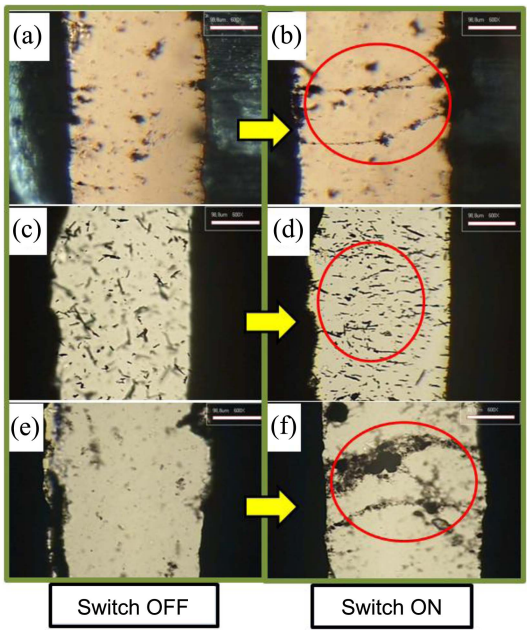

Figure 9. Optical microscopic images of the carbons dispersed in silicone oil before (left) and after the application of an electric field strength of 1.4 kV/mm (at the same weight loading of carbons). Both sides of the horizontal black stripes represent the electrodes. The gap distance between two parallel electrodes was 350 mm. (a and b; CNT, c and d; CMK3, e and f; CNT/CMK3)

The sample formed thin and dense chains of particles under the applied electric field within 1 sec, and the structure remained stable as long as the field was applied. Fibrillated chains were observed and spanned between two electrodes. Thick chains formed under the application of an electric field in the CNT/CMK3 dispersed solution (Fig. 9(f)). On the other hand, the CNTs formed very thin rows perpendicular to the electrodes (Fig. 9(b)), but the carbon particles of the CMKs aligned like dotted lines indicating poor electrical conductivity (Fig. 9(d)). The fibrillated chains structure might provide a path for the transporting of mobile carriers, which would determine the conducting behavior of ER fluids. The electrical conductivity of the CNT/CMK3 composite was superior to each individual carbon sample, such as CNT and CMK3. This was attributed to the outer shape of the CNT/CMK3 having a sea urchin like appearance.

Figure 10 shows the cyclic voltammograms of the CNTs, CMK3 and CNT/CMK3 in 1 M H_2SO_4. The electrode displays a capacitive charging current in both (anodic and cathodic) scanning directions across the potential range, 0.2 V to 0.8 V (*versus* Ag/AgCl reference electrode) at a scan rate of 70 mV/s. The redox current intensity of the CNT/CMK3 composite was much higher than that of CMK3 and the commercial CNTs. This suggests that CNT/CMK3 has a unique structure with a high surface area, large pore size and high electronic conductivity, which can provide fast, stable, reversible faradaic reactions. On the other hand, the capacitive charging current was increased by the KOH treatment of the carbon samples due to the development of porosity, as can be seen in Figure 10.

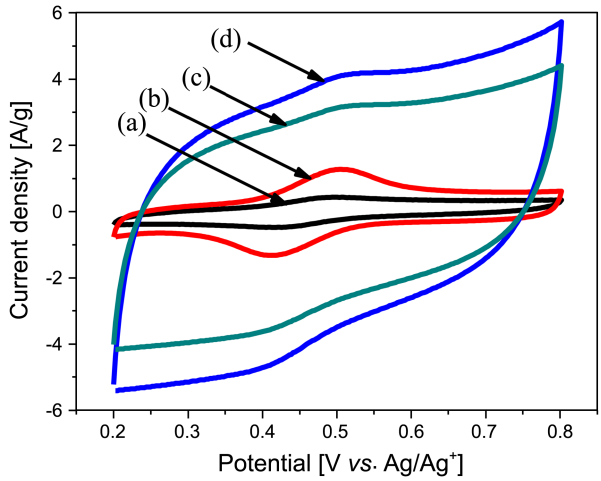

Figure 10. Cyclic voltammograms of commercial MWCNT (a), 20 wt % KOH modified CNT (b), CNT/CMK3 composite (c), KOH modified CNT/CMK3 composite (d) in 1 M H_2SO_4 at scan rate of 70 mV/s.

The CVs of the mesoporous carbon hollow spheres maintained symmetrical rectangular shape at all voltage sweep rates, ranging from 30 to 100 mVs^{-1}, indicating excellent capacitive behavior even at a very fast sweep rate. This will lead to a better understanding of the actual participation of the CNT/CMK3 electrode in the redox process.

The enhanced thermal conductivity of the polymer composites using CNT is an attractive research area.[27] In this study, the pristine commercial MWCNT, mesoporous CMK3 or CNT/CMK3 composite were incorporated in the polymethyl methacrylate (PMMA) matrix. The fabricated PMMA-carbon composites showed improved thermal conductivity and electrical conductivity. The thermal conductivity of the prepared silicone pads was measured quickly using a hot wire method. The thermal conductivity can be obtained using the following equation:

$$\lambda = \frac{q \cdot \ln(t2/t1)}{4\pi(T2-T1)}$$

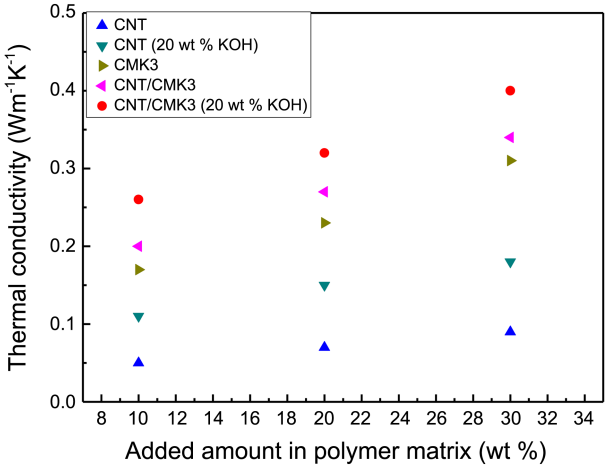

Figure 11. Thermal conductivity vs. carbon additive concentration with 10-30 wt % to PMMA.

where λ is the thermal conductivity of the sample and q is the heat per unit length generated. T and t are the temperature and time, respectively.[27]

Figure 11 shows the thermal conductivity of the composites filled with 10, 20 and 30 wt % MWCNT, CMK3 or CNT/CMK composite to PMMA. The thermal conductivity of the MWCNT-incorporated composites increased progressively with increasing CNT/CMK3 concentration up to 30 wt % to PMMA. The thermal conductivity of 10, 20 and 30 wt % CNT/CMK3-incorporated PMMA was 0.201, 0.273 and 0.339 $Wm^{-1} K^{-1}$, respectively. At 10 wt % pure CMK3 to PMMA, the thermal conductivity of the polymer composite was 0.172 $Wm^{-1} K^{-1}$. At the same carbon filler content, the PMMA composite filled with 10 wt % pure CMK3 to PMMA showed a 340% higher thermal conductivity than that of the 10 wt % CNT only filled composite. A good dispersion of carbon in the polymer matrix is vital for improving the thermal conductivity. Excellent dispersibility was achieved when CMK3 or CNT/CMK3 was incorporated in the polymer, compared to pristine CNT. In addition, higher thermal conductivity was obtained when the KOH-modified carbon composites were used instead of pristine CNT or CNT/CMK3. The thermal conductivity increased from 0.264 $Wm^{-1} K^{-1}$ to 0.325 $Wm^{-1} K^{-1}$ with increasing KOH loading from 20 wt % to 30 wt %, at a 10 wt % carbon filler content in PMMA. The superior thermal conduction behavior of the CMK3- and CNT/CMK-containing PMMA was attributed to their high absorption capacity and dispersibility. In particular, for the CNT/CMK3 composite, the unique apparent structure of the CNTs tangled and stretched out from the surfaces of CMK3 can improve the thermal conductivity.

Conclusions

Composite materials of mesoporous carbon and carbon nanotubes were synthesized using Ni, Co and Pd-loaded CMK3 *via* the catalytic reaction of methane and CO_2. The CNTs grew from the pores of mesoporous carbon. The CNTs were attached tightly to the surfaces of CMK3 in a densely tangled shape. The CNT/CMK3 composite exhibited both non-graphitic mesoporous structures and the graphitic characteristics originating from the MWCNTS in the pores of CMK3. In contrast, carbon fibers formed instead of carbon tubes when Pd was used as a catalyst, showing no vacant channels in the carbon bodies. The electrochemical properties of the materials were characterized by observing the electrorheological (ER) effects and cyclic voltammetry. The composites of CNTs and mesoporous carbon showed a higher electrical conductivity and current density. CNT/CMK3 or KOH-modified CNT/CMK3 particles were incorporated in the PMMA matrix to improve the thermal conductivity. The thermal conductivity of the PMMA composites increased with increasing CNT/CMK3 content. Higher thermal conductivity was achieved when the KOH-modified carbon composites were used instead of pristine CNT or CNT/CMK3. The superior thermal and electrical conduction behavior of CMK3 and the CNT/CMK3 composite was attributed to their high absorption capacity and dispersibility. For the CNT/CMK3 composite, the unique sea urchin like structure resulted in improved thermal conduction. Overall, the CNT/CMK3 carbon composites are expected to find applications as advanced electrode materials in electrochemistry.

Acknowledgments. This research was supported in part by Research grant from Inha University in 2013 and by a New & Renewable Energy of the Korea Institute of Energy Technology Evaluation and Planning (KETEP) grant funded by the Korea government Ministry of Knowledge Economy (No. 20113030040010).

References

1. Li, H.; Wang, R.; Cao, R. *Microporous and Mesoporous Materials* **2008**, *111*, 32.
2. Lei, Y.; Fournier, C.; Pascal, J.-L.; Favier, F. *Microporous and Mesoporous Materials* **2008**, *110*, 167.
3. Ko, J. M.; Kim, K. M. *Materials Chemistry and Physics* **2009**, *114*, 837.
4. Raymundo-Pinero, E.; Khomenko, V.; Frackowiakm, E.; Beguin, F. *J. Electrochem. Soc.* **2005**, *152*, A229.
5. Wang, G.-X.; Zhang, B.-L.; Yu, Z.-L.; Qu, M.-Z. *Solid State Ionics* **2005**, *176*, 1169.
6. Fan, Z.; Chen, J.; Wang, M.; Cui, K.; Zhou, H.; Kuang, Y. *Diamond Relat. Mater.* **2006**, *15*, 1478.
7. Subramanian, V.; Zhu, H.; Wei, B. *Electrochem. Commun.* **2006**, *8*, 827.
8. Fuertes, A. B.; Lota, C.; Centeno, T. A.; Frackowiak, E. *Electrochim. Acta* **2005**, *50*, 2799.
9. Han, S.; Hyeon, T. *Chem. Commun.* **1999**, *19*, 1955.
10. Han, S.; Lee, K.; Oh, S.; Hyeon, T. *Carbon* **2003**, *41*, 1049.
11. Yu, J.; Yoon, S. B.; Chai, G. S. *Carbon* **2001**, *39*, 1442.
12. Toupin, M.; Blanger, D.; Hill, I. R.; Quinn, D. *J. Power Sources* **2005**, *140*, 203.
13. Barisci, J. N.; Wallace, G. G.; Baughman, R. H. *J. Electrochem. Soc.* **2000**, *147*, 4580.
14. An, K. H.; Kim, W. S.; Park, Y. S.; Choi, Lee, S. M.; Chung, D. C.; Bae, D. J.; Lim, S. C.; Lee, Y. H. *Adv. Mater.* **2001**, *13*, 497.
15. Ma, R. Z.; Liang, J.; Wei, B. Q.; Zhang, B.; Xu, C. L.; Wu, D. H. *J. Power Sources* **1999**, *84*, 126.
16. Diederich, L.; Barborini, E.; Piseri, P.; Podesta, A.; Milani, P.; Schneuwly, A.; Gallay, R. *Appl. Phys. Lett.* **1999**, *75*, 2662.
17. An, K. H.; Kim, W. S.; Park, Y. S.; Moon, J.-M.; Bae, D. J.; Lim, S. C.; Lee, Y. S.; Lee, Y. H. *Adv. Functional Mater.* **2001**, *11*, 387.
18. Peigney, A.; Laurent, Ch.; Flahaut, E.; Rousset, A. *Carbon* **2001**, *39*, 507.
19. An, K. H.; Jeon, K.; Heo, J.; Lim, S.; Bae, D.; Lee, Y. *J. of Electrochem. Soc.* **2002**, *149*, A1058.
20. Jurewicz, K.; Delpeux, S.; Bertagna, V.; Beguin, F.; Frackowiak, E. *Chem. Phys. Lett.* **2001**, *347*, 36.
21. Park, J.; Ko, J.; Park, O. *J. of Electrochem. Soc.* **2003**, *150*, A864.
22. Dong, X.; Shen, W.; Gu, J.; Xiong, L.; Zhu, Y.; Li, H.; Shi, J. *J. Phys. Chem. B* **2006**, *110*, 6015.
23. Jun, S.; Joo, S. H.; Ryoo, R.; Kruk, M.; Jaroniec, M.; Liu, Z.; Ohsuna, T.; Terasaki, O. *J. Am. Chem. Soc.* **2000**, *122*, 10712.
24. Fuertes, A. B.; Alvarez, S. *Carbon* **2004**, *42*, 3049.
25. Obraztsov, A. N.; Obraztsova, E. A.; Tyurnina, A. V.; Zolotukhin, A. A. *Carbon* **2007**, *45*, 2017.
26. Guo, X.-F.; Kim, J.-H.; Kim, G-J. *Catal. Tod.* **2011**, *164*, 336.
27. Hong, J.; Lee, J.; Jung, D.; Shim, S. E. *Thermochimica Acta* **2011**, *512*, 34.